



**HAL**  
open science

## Improved frequency comb operation of an InAs/GaAs hybrid multisection quantum dot laser on silicon

Thibaut Renaud, Heming Huang, G Kurczveil, D Liang, R G Beausoleil,  
Frédéric Grillot

► **To cite this version:**

Thibaut Renaud, Heming Huang, G Kurczveil, D Liang, R G Beausoleil, et al.. Improved frequency comb operation of an InAs/GaAs hybrid multisection quantum dot laser on silicon. Applied Physics Letters, 2023, 123 (1), pp.011105:1-011105:6. 10.1063/5.0143570 . hal-04555341

**HAL Id: hal-04555341**

**<https://telecom-paris.hal.science/hal-04555341>**








Submitted on 22 Apr 2024

**HAL** is a multi-disciplinary open access archive for the deposit and dissemination of scientific research documents, whether they are published or not. The documents may come from teaching and research institutions in France or abroad, or from public or private research centers.

L'archive ouverte pluridisciplinaire **HAL**, est destinée au dépôt et à la diffusion de documents scientifiques de niveau recherche, publiés ou non, émanant des établissements d'enseignement et de recherche français ou étrangers, des laboratoires publics ou privés.

RESEARCH ARTICLE | JULY 06 2023

## Improved frequency comb operation of an InAs/GaAs hybrid multisection quantum dot laser on silicon

T. Renaud ; H. Huang ; G. Kurczveil ; D. Liang ; R. G. Beausoleil ; F. Grillot  



*Appl. Phys. Lett.* 123, 011105 (2023)

<https://doi.org/10.1063/5.0143570>

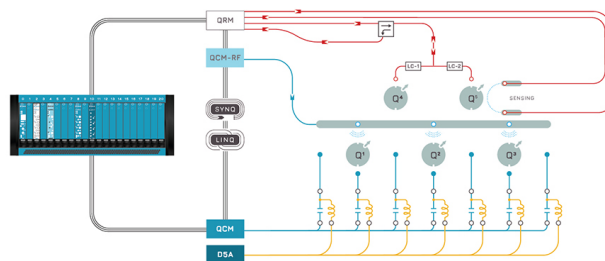


CrossMark

 QBLOX

Integrates all  
Instrumentation + Software  
for Control and Readout of

**Superconducting Qubits**  
**NV-Centers**  
**Spin Qubits**



Spin Qubits Setup

[find out more >](#)

# Improved frequency comb operation of an InAs/GaAs hybrid multisection quantum dot laser on silicon

Cite as: Appl. Phys. Lett. **123**, 011105 (2023); doi: [10.1063/5.0143570](https://doi.org/10.1063/5.0143570)

Submitted: 24 January 2023 · Accepted: 16 June 2023 ·

Published Online: 6 July 2023









View Online



Export Citation



CrossMark

T. Renaud,<sup>1</sup>  H. Huang,<sup>1</sup>  G. Kurczveil,<sup>2</sup>  D. Liang,<sup>2</sup>  R. G. Beausoleil,<sup>2</sup>  and F. Grillot<sup>1,3,a)</sup> 

## AFFILIATIONS

<sup>1</sup>Télécom Paris, Institut Polytechnique de Paris, 19 Place Marguerite Perey, Palaiseau 91120, France

<sup>2</sup>Large-Scale Integrated Photonics Lab, Hewlett Packard Labs, Hewlett Packard Enterprise, Milpitas, California 95035, USA

<sup>3</sup>Center for High Technology Materials, University of New-Mexico, 1313 Goddard SE, Albuquerque, New Mexico 87106, USA

<sup>a)</sup> Author to whom correspondence should be addressed: [frederic.grillot@telecom-paris.fr](mailto:frederic.grillot@telecom-paris.fr)

## ABSTRACT

This work reports on a systematic investigation of the frequency comb enhancement in hybrid InAs/GaAs multisection quantum dot lasers on silicon. The colliding configuration provides an operating frequency at twice the fundamental frequency of the free-spectral range of the cold cavity. In particular, the contribution of the linewidth enhancement factor, or  $\alpha_H$ -factor, on the comb formation is investigated with respect to the reverse voltage and temperature conditions. When those parameters are varied, the formation of the combs is found to increase with respect to  $\alpha_H$ . In addition, we also demonstrate that this quantum dot laser exhibits a comb behavior, while the beatnote locking is not fully achieved. This effect is essentially due to the dispersion which is not fully compensated from the optical nonlinearities. These results bring further insights on comb and pulse formations in multisection quantum dot lasers, which is important for designing future light sources for on-chip and chip-to-chip optical interconnects.

Published under an exclusive license by AIP Publishing. <https://doi.org/10.1063/5.0143570>

Artificial intelligence (AI) and deep-learning technologies are nowadays profoundly tied with our daily life. With the expansion of the telecom infrastructure as well as active devices that are connected to the Internet in the billions each year,<sup>1</sup> algorithmic models are scaling up to properly handle the surging data clusters. For instance, Google is training a deep-learning-based model of  $100 \times 10^{12}$  parameters.<sup>2</sup> On this front, high-performance computing (HPC) is the key unlocking promised perspectives. Nevertheless, modern computers are based on von Neumann architecture, i.e., separated memory units (where instructions and data are stored) and processing units (where operations are executed), and frequent communications between these system components are creating struggles for hardware to keep up with the pace of programming advance, as moving data back and forth on board not only generates performance-limiting latency but also can cost more than 100 times more energy than a simple add operation.<sup>3,4</sup> Considerable efforts have been devoted to increasing system energy efficiency from different approaches, such as in-memory computation, smarter algorithm, and power management.<sup>5,6</sup> Nevertheless, on-chip or off-chip information access still relies on electric wiring. To this end, using optical interconnects as an alternative data pipeline has

become an attractive solution: with proper optical waveguides, light propagation is less lossy and does not generate extra heat. Moreover, combined with integrated dense wavelength-division multiplexing (DWDM) based on photonic integrated circuits (PICs), such approach allows not only to speed up HPC in chip-to-chip transmission capacity but also to elevate system efficiency by reducing redundant FPGA footprints. On this stage, the multiple-wavelength channels can be generated either by combining a series of single-wavelength lasers or by considering a single laser producing a wide optical frequency comb (OFC).<sup>7</sup> Compared to the former, the OFC option offers straightforward advantages: instead of stacking several laser sources together, only one laser is enough to handle the task, thus, less energy is required for light generation and cooling, and the device can be rendered in a much more compact design. In addition, OFC offers stabilized free spectral range (FSR), i.e., fixed channel spacing with narrow linewidth. To achieve this goal, quantum dots (QDs) are considered as an ideal material candidate to achieve these perspectives. Owing to their three-dimensional carrier-confining nanostructure nature, QD lasers exhibit atom-like behavior and a discretized density of states, leading to high thermal stability, low threshold current density, ultrafast carrier

dynamics, and less fluctuations of both phase and intensity noises,<sup>8–12</sup> thus reconciling all the most sought-after qualifications for an on-chip laser device. Furthermore, dot size dispersion is often encountered during growth of QD, leading to an inhomogeneously broadened gain spectrum that is beneficial for reaching wide-span OFC generation. Last but not least, external optical feedback effects in semiconductor lasers heavily depend on material and cavity design properties; however, QD lasers have been shown to be much more resilient against such reflections.<sup>13</sup> This property makes them attractive for silicon integration as unwanted optical feedback is problematic for PICs, and no both effective and low-cost integrable optical isolator is yet available.

A comb laser produces a coherent dynamical regime, consisting of a sequence of equally spaced lines in the frequency domain, characterized by relatively low intensity and phase noise. The phase correlation occurring between the modes of a comb distinguishes this class of regimes from an array of equally spaced lines emitted by different lasers and implies a dual representation in time domain as a perfectly periodic waveform. The comb operation is usually obtained when considering a two-section mode-locked laser (MLL), whereby a nonlinear element that is to say a saturable absorber (SA) placed at the edge of the laser cavity can also produce pulse generation, which occurs when the gain becomes larger than the loss resulting in positive net gain. However, the comb generation is more subtle since the SA needs to be well-dimensioned for pulse generation and relocated from the edge to generate higher-order-harmonics of the cavity resonance. On this stage, the SA plays a leading role in engineering the spectral properties of OFC. In this paper, we qualitatively investigate how the saturable absorption impacts on the comb profile, by considering two hybrid InAs/GaAs QD comb lasers developed on silicon with identical epilayer structures from the same wafer run, the only difference between being whether the SA is present or not. Experimental results unveil that one of the bridging parameters between SA and OFC profile is the linewidth enhancement factor, or  $\alpha_H$ -factor, where a higher value is found beneficial in broadening the entire comb envelope.<sup>14,15</sup> On the top of that, the experiments confirm the possibility to achieve comb operation without pulses as a direct consequence of the background dispersion. We believe that these experiments bring further insights on engineering efficient comb sources for future integrated DWDM solutions used in short-reach transmissions and HPC applications.

The formation of frequency combs and pulse train formation can be analyzed through the intracavity electric field,

$$E(z, t) = \sum_n E_n(t) \cos \varphi_n(t) u_n(z), \quad (1)$$

where  $u_n(z)$  is the passive cavity modes of the resonator, while  $E_n(t)$  and  $\varphi_n(t)$  account for the mode amplitude and phase, respectively. Therefore, the frequency comb is developed when the following condition is satisfied,

$$\varphi_n(t) = (f_0 + nf_r)t + \phi_n, \quad (2)$$

with  $f_0$  being the carrier-envelope offset frequency and  $\phi_n$  being the phase of each longitudinal mode. On the one hand, an OFC is defined as a coherent radiation characterized by a spectrum consisting of a set of modes equally spaced and presenting a phase relationship between each other. The repetition rate  $f_r$  associated with the beatnote locking is, thus, determined by the cavity length through such as  $f_r = v_g/2L_c$ , with  $v_g$  the group velocity of the light and  $L_c$  the length of the laser

cavity. As recently shown in quantum cascade lasers (QCLs), the  $\alpha_H$ -factor was found to play a significant role in the comb dynamics. A non-zero  $\alpha_H$  was found necessary for producing a multimode instability with straightforward implications in the formation of frequency-modulated combs in Fabry-Pérot QCLs.<sup>16,17</sup> In other papers, the effective value given by  $\alpha_{He} = \sqrt{1/\Delta\nu \times \int_{comb} \alpha_H^2(\nu') d\nu'}$  was directly connected to the comb envelope  $\Delta\nu$ .<sup>15</sup> On the other hand, when phase-locking of the modes is achieved such that  $\phi_0 = \phi_1 = \phi_2 = \dots$ , mode-locking dynamics occurs along with a pulse train. However, it is known that the quality of a pulse is usually affected by the group velocity dispersion (GVD), meaning that the group velocity changes for different wavelengths in the pulse. This critical parameter that originates from different contributions (waveguide, material, and gain properties) can be minimized through a careful control of the QD size uniformity leading to a near-zero  $\alpha_H$  factor.<sup>18</sup> Overall, the occurrence of pulses in the mode-locking regime is balanced between the GVD and the optical nonlinearities originating from saturable absorption and 4-wave mixing. If the optical nonlinearities do not overcome the GVD, the pulses are altered or can even be completely suppressed leading to comb dynamics without pulses. On the contrary, when the 4-wave mixing is strong as in QD materials,<sup>19</sup> even a single gain section is able to produce mode-locking with sub-picosecond pulses.<sup>20,21</sup>

The QD comb laser under study is schematically shown in Fig. 1. The structure consists of a long cavity  $L_c = 2.6$  mm that has mirrors with 50% reflectivity on one side and 100% on the other, and a 1.4-mm-long active region is placed in the center. The semiconductor optical amplifier (SOA) section incorporates eight layers of QDs, and one of the two lasers has a 176- $\mu\text{m}$ -long SA positioned in the middle in order to favor the frequency comb operation. Another QD laser without SA is used as a reference. Anterior works already showed that this colliding configuration is powerful for generating harmonics mode-locking.<sup>22–24</sup> From a general viewpoint, the position of SA in a MLL is a decisive parameter in selecting higher-order harmonics associated with the fundamental frequency, which is basically analogue to the method used by a violinist to create high order harmonic sounds. Therefore, the strumming of the violin without the violinist placing a finger upon the fingerboard creates the first harmonic also known as the fundamental harmonic. If the location of the node is in the center of the fingerboard, this results in the creation of the second harmonic, which is exactly similar to the colliding configuration of the QD comb laser under study. Finally, mode converters ensure the optical mode transfer from active waveguide down to the passive Si waveguide, and the output light is coupled out through a grating coupler (GC).

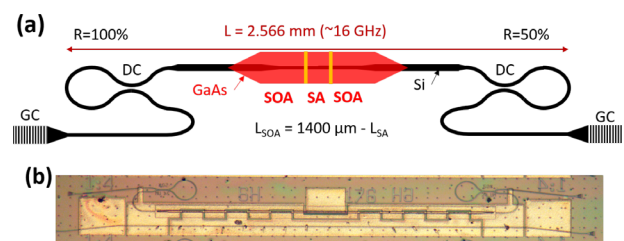


**FIG. 1.** (a) Schematics of the laser cavity design (SOA: semiconductor optical amplifier; SA: saturable absorber; GC: grating coupler; DC: directional coupler). (b) Microscope picture of a similar device.

The hybrid integration is realized by wafer-bonding the unpatterned wafer of InAs/GaAs QDs on a silicon-on-insulator (SOI) wafer with the passive Si structures already patterned. Standard III-V processing techniques are then performed to etch the InAs/GaAs waveguide and deposit the metal contacts. More information about the epitaxial process and laser fabrication can be found elsewhere.<sup>25,26</sup> Two Sagnac loops with directional couplers (DC) constitute the mirrors of the cavity. Outside the mirrors, after an integrated external cavity with an effective length four times smaller than the main cavity, the light is vertically out-coupled through a grating coupler (GC) into a micro-lensed optical fiber. The total cavity length leads to a fundamental frequency of  $f_r = 16$  GHz.

Figure 2 shows the 20 °C light-current characteristics of the QD comb lasers for different reverse voltage conditions  $V_{SA} = 0V, -4V,$  and  $-6V$ , the reference QD laser being displayed in blue for comparison. The threshold current increases from 23 to 29 mA when the reverse voltage varies from 0 to  $-6V$ , by comparison with the reference laser, which exhibits a threshold at 16 mA. This effect is attributed to the higher saturable loss induced by the carrier sweep-out time that decreases as the reverse-bias voltage is increased. It also causes the output power to decrease with the increasing reverse voltage. The reference laser, however, displays a lower output power, which might stem from slight imperfections in the fabrication, especially in the mirrors.

Figures 3(a) and 3(b) show the  $2 \times I_{th}$  optical spectra of the laser with SA, at 20 °C for  $V_{SA} = 0$  and  $-4V$ . The emission is centered, respectively, around 1296 and 1297.5 nm, and it can be noted that the comb is not yet formed at 0 V, while it does at  $-4V$ , with four modes within the  $-10$  dB bandwidth. In our experiments, the presence of the frequency comb is identified via two criteria: whether the recorded RF spectrum shows a clear beatnote that is relevant to the SA positioning, and whether the optical spectrum displays a corresponding FSR between the optical modes arisen from the noise floor.

Figure 4 similarly shows the comb of the laser with SA at  $2 \times I_{th}$  and  $V_{SA} = -6V$ , for temperatures of 20, 30, 40, and 50 °C. The number of modes within the  $-10$  dB bandwidth is, respectively, 6, 8, 11, and 12, which highlights the increase in the comb width with the temperature. The contributions to the thermal expansion of the comb can be attributed to multiple mechanisms: intensifying carrier thermalization that favors stronger carrier-carrier scattering and faster gain recovery, expanding homogeneous broadening that couples more originally non-radiative quantum dot groups as well as rising of the

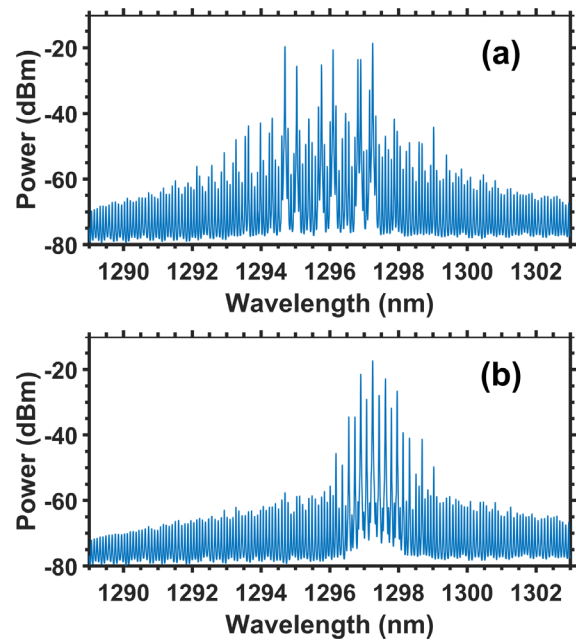


FIG. 3. Optical spectra of the QD laser with SA at 20 °C for bias conditions of  $2 \times I_{th}$  and (a)  $V_{SA} = 0V$  and (b)  $V_{SA} = -4V$ .

$\alpha_H$ -factor that enhances four-wave mixing effects.<sup>27</sup> Furthermore, it is important to stress that this increase is not symmetric, since the comb spreading is more pronounced at longer wavelengths, which means that larger dots are preferentially activated. Hereinafter, the  $\alpha_H$ -factor is extracted for each comb line from the measurement of the amplified spontaneous emission (ASE), which is performed from optical spectra measured at different sub-threshold currents.<sup>28</sup> The  $\alpha_H$  is related to the differential gain  $dg/dI$  and to the carrier-induced modal blue-shift  $d\lambda_c/dI$ , through  $\alpha_H = -\frac{4n\pi}{\lambda^2} \times \frac{d\lambda_c/dI}{dg/dI}$ , where  $n$  is the effective group index and  $\lambda$  is the photon wavelength.<sup>29,30</sup> First, the net modal gain is calculated using the ASE spectrum, and the differential gain  $dg/dI$  is obtained by taking the slope of  $g(I)$  below threshold. The corresponding modal wavelength shift is also determined after that thermal effects resulting in a red-shift are properly eliminated. As the gain is clamped above threshold, only the thermal effects remain, and their impacts on

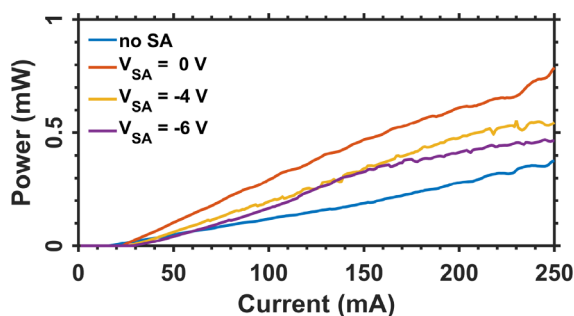


FIG. 2. Room temperature light-current characteristics of the QD comb lasers under different SA voltages. The configuration without SA is reported (blue).

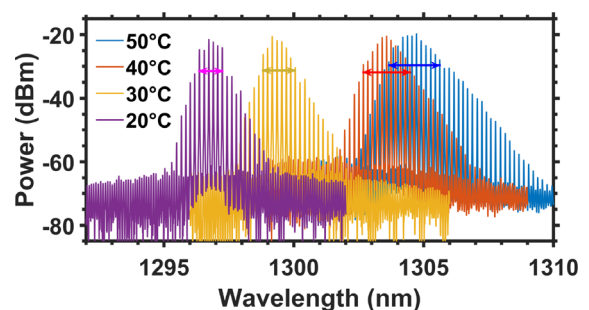


FIG. 4. Optical spectra of the QD laser with SA at  $2 \times I_{th}$  and  $V_{SA} = -6V$ , for temperatures from 20 to 50 °C. The arrows represent the  $-10$  dB bandwidths.



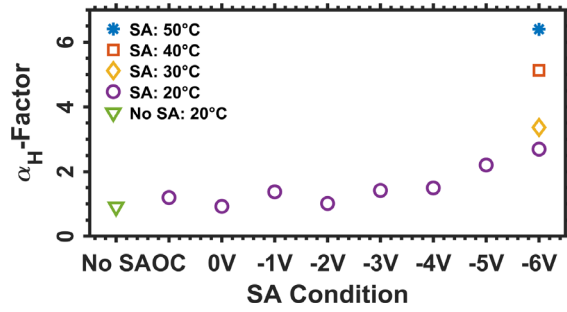


FIG. 5. The  $\alpha_H$ -factor measured at threshold around the first lasing mode of both QD comb lasers under different SA and temperature conditions. OC stands for open circuit.

the modal wavelength can be measured from the slope above threshold and then removed from the below-threshold wavelength shift.

For  $V_{SA} = -6V$ , the extraction of the  $\alpha_H$ -factor was performed at 30, 40, and 50 °C. Figure 5 shows the spectral dependence taken around the first lasing mode, i.e., the mode with the highest intensity just above threshold for each condition. Without SA, the  $\alpha_H$  reaches its lowest value at around 0.9 and increases subsequently to 1.2 when the SA is included but left open [open circuit (OC)]. This change is attributed to the higher losses in the SA, which also further explains the slight increase from 0.92 at 0 V to 1.5 at -4 V. Beyond -4 V, the  $\alpha_H$  significantly scales up with the increasing SA voltage, reaching up to 2.7 at -6 V. Interestingly, the increase in the  $\alpha_H$ -factor at high reverse bias appears to result in a broader comb.<sup>31</sup> For instance, Figs. 3(a) and 3(b) show the spectra at  $2\times$  the threshold, where the comb is not formed at  $V_{SA} = 0V$  with lasing modes quite randomly distributed, while it is starting to be formed at -4 V. When increasing the temperature results in a similar increase in the  $\alpha_H$  from 2.7 at 20 °C to 6.4 at 50 °C. At 50 °C, Fig. 4 shows the comb completely formed for  $V_{SA} = -6V$ , which corresponds to the SA voltage for which the highest value of  $\alpha_H$ -factor was measured.

Furthermore, Fig. 6 displays the corresponding RF beatnotes for the combs between 20 and 50 °C. The central frequency is around 31.5 GHz, hence corresponding to twice the FSR of the cavity resonance. As aforementioned, it does confirm that the comb laser operates on the second harmonic. This effect is also visible in the optical spectra [Figs. 3(b) and 4], which show alternates between lasing and suppressed comb lines. Surprisingly, the RF linewidth is found quite

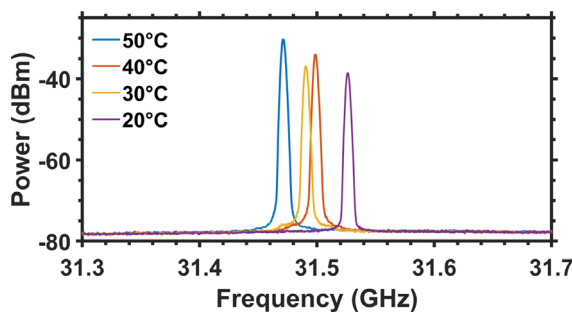


FIG. 6. RF beatnote of the QD laser with SA at  $2 \times I_{th}$  and  $V_{SA} = -6V$ , for temperatures between 20 and 50 °C.

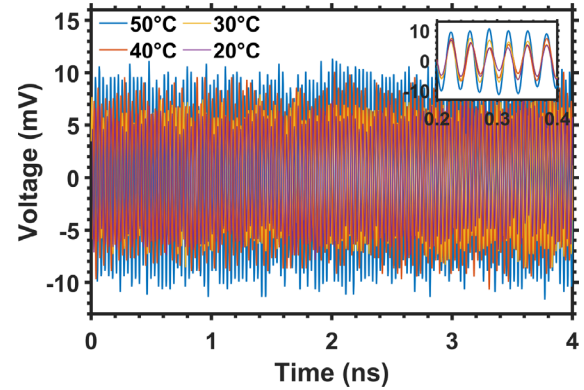


FIG. 7. Temporal trace of the QD laser with SA at  $2 \times I_{th}$  and  $V_{SA} = -6V$ , for temperatures between 20 and 50 °C. The inset shows a zoom between 0.2 and 0.4 ns.

large at 3 MHz regardless the temperature, hence, proving that the beatnote locking is not fully achieved. Based on these experiments, it is important to note that no transition between locked and unlocked regimes was observed. Thus, by sweeping the operating conditions, a comb formation pops-up, but this formation always results from a broad beatnote. By comparison, mode-locked operation exhibiting pulses results in beatnote of a few hundreds of kHz.<sup>32</sup> As a consequence, no short pulses are observed in the time series displayed in Fig. 7. Whatever the temperature, the time traces exhibit rather near-sinusoidal oscillations as illustrated by the inset of Fig. 7. The mean amplitude of the oscillations increases with the temperature, from 11.7 mV at 20 °C to 19.3 mV at 50 °C. The values of the  $\alpha_H$ -factor, the number of lines in the -10 dB bandwidth (as identified by the arrows in Fig. 4), the peak power of the RF beatnote in Fig. 6, and the mean amplitude of the oscillations in Fig. 7 are all summarized in Table I for the studied temperatures of 20, 30, 40, and 50 °C.

As aforementioned, the presence of oscillations instead of clear pulses results in an incomplete phase-locking due to the fact that the GVD is not fully compensated by the optical nonlinearities. Other assumptions could be attributed to a phase unlocked multimode regime<sup>33</sup> or to a large variation of the  $\alpha_H$  across the different sections that could result in phase instabilities in the pulse train.<sup>34,35</sup> Yet, in our case, expected frequency comb profile can only be found at high SA voltage, without any sign of unstable pulses in the time traces, which can also be confirmed by the steady beatnote linewidth. Last but not the least, it has to be stressed that the absence of pulses in DWDM applications is an advantageous feature: indeed, a constant-output power has a lower risk of triggering unwanted nonlinearities further down-link and contributes to increase device reliability.<sup>7</sup>

TABLE I. Summary of results at the different temperatures.

Temperature	20 °C	30 °C	40 °C	50 °C
SA voltage (V)	-6	-6	-6	-6
$\alpha_H$ -factor	2.7	3.4	5.1	6.4
# of lines within 10 dB power variation	6	8	11	12
RF beatnote power (dBm)	-38.5	-36.8	-33.9	-30.1
Mean amplitude of oscillations (mV)	11.7	12.4	16	19.3

To conclude, hybrid InAs/GaAs QD comb lasers with and without SA are studied in this work. When the SA is present, the operating frequency equals twice the cavity FSR as a consequence of the second-harmonic induced from the colliding configuration. The  $\alpha_H$ -factor is measured with varying SA and temperature conditions. The frequency comb operation is analyzed from optical and RF spectra along with time series. The results show that both high reverse bias voltage on the SA and high temperature contribute to increase the  $\alpha_H$ -factor, hence setting the stage in favor of the comb broadening. As a result of an incomplete mode-locking, no pulses are observed in the time domain, which is confirmed from the large beatnote. This work highlights that when optical nonlinearities do not fully compensate for dispersion, frequency combing can occur without pulse generation. However, care must be taken because frequency-modulated (FM) combs can also lead to the same behavior without SA hence prohibiting the emission of pulses. In this case, the OFC operation is characterized by a nearly constant optical power and a strong periodic modulation of the instantaneous frequency. The phase difference between adjacent modes is therefore constant in time, but not equal for each couple of modes which is exactly what happens in the FM combs emerging without any SA in QD lasers and QCLs. This work brings addition information on the comb and pulse formation in multisected QD devices, which are meaningful for the conception of integrated constant-output large-comb DWDM laser sources. Further work will now investigate line-width and phase properties across the comb spectrum.

The authors would like to thank Hewlett-Packard Enterprise and the Institut Mines Telecom for financial support of this work.

## AUTHOR DECLARATIONS

### Conflict of Interest

The authors have no conflicts to disclose.

### Author Contributions

**Thibaut Renaud:** Data curation (lead); Investigation (equal); Writing – original draft (lead); Writing – review & editing (equal). **Heming Huang:** Data curation (supporting); Investigation (equal); Supervision (supporting); Writing – original draft (equal); Writing – review & editing (equal). **Geza Kurczveil:** Conceptualization (supporting); Investigation (supporting); Writing – original draft (supporting); Writing – review & editing (equal). **Di Liang:** Conceptualization (supporting); Investigation (supporting); Writing – review & editing (equal). **Ray Beausoleil:** Conceptualization (supporting); Formal analysis (equal); Supervision (supporting); Writing – review & editing (supporting). **Frederic Grillot:** Investigation (equal); Supervision (equal); Writing – original draft (equal); Writing – review & editing (equal).

### DATA AVAILABILITY

The data that support the findings of this study are available from the corresponding author upon reasonable request.

### REFERENCES

<sup>1</sup>“Current IoT forecast highlights,” Technical Report, Transforma Insights, 2022.

- <sup>2</sup>C. Zhang and C. Mezzanotte, “Training deep learning-based recommender models of 100 trillion parameters over Google Cloud,” Technical Report, Google Cloud, 2022.
- <sup>3</sup>D. Pandiyani and C.-J. Wu, “Quantifying the energy cost of data movement for emerging smart phone workloads on mobile platforms,” in *2014 IEEE International Symposium on Workload Characterization (IISWC)* (IEEE, 2014), pp. 171–180.
- <sup>4</sup>O. Mutlu, S. Ghose, J. Gómez-Luna, and R. Ausavarungrun, “Processing data where it makes sense: Enabling in-memory computation,” *Microprocess. Microsyst.* **67**, 28–41 (2019).
- <sup>5</sup>M. S. Q. Zulkar Nine, L. Di Tacchio, A. Imran, T. Kosar, M. F. Bulut, and J. Hwang, “Greendataflow: Minimizing the energy footprint of global data movement,” in *2018 IEEE International Conference on Big Data (Big Data)* (IEEE, 2018), pp. 335–342.
- <sup>6</sup>B. Feinberg, B. C. Heyman, D. Mikhailenko, R. Wong, A. C. Ho, and E. Ipek, “Commutative data reordering: A new technique to reduce data movement energy on sparse inference workloads,” in *2020 ACM/IEEE 47th Annual International Symposium on Computer Architecture (ISCA)* (IEEE, 2020), pp. 1076–1088.
- <sup>7</sup>G. Kurczveil, Y. Yuan, J. Youn, B. Tossoun, Y. Hu, S. Mathai, P. Sun, J. Hulme, and D. Liang, “Innovative DWDM silicon photonics for high-performance computing,” in *Silicon Photonics for High-Performance Computing and Beyond* (CRC Press, 2021), pp. 191–221.
- <sup>8</sup>D. Bimberg, “Quantum dot based nanophotonics and nanoelectronics,” *Electron. Lett.* **44**, 168 (2008).
- <sup>9</sup>D. Deppe, K. Shavritranuruk, G. Ozgur, H. Chen, and S. Freisem, “Quantum dot laser diode with low threshold and low internal loss,” *Electron. Lett.* **45**, 54–56 (2009).
- <sup>10</sup>P. Borri, W. Langbein, J. M. Hvam, F. Heinrichsdorff, M.-H. Mao, and D. Bimberg, “Ultrafast gain dynamics in InAs-InGaAs quantum-dot amplifiers,” *IEEE Photonics Technol. Lett.* **12**, 594–596 (2000).
- <sup>11</sup>D. Gready, G. Eisenstein, C. Gilfert, V. Ivanov, and J. P. Reithmaier, “High-speed low-noise InAs/InAlGaAs/InP 1.55- $\mu\text{m}$  quantum-dot lasers,” *IEEE Photonics Technol. Lett.* **24**, 809–811 (2012).
- <sup>12</sup>J. Duan, X.-G. Wang, Y.-G. Zhou, C. Wang, and F. Grillot, “Carrier-noise-enhanced relative intensity noise of quantum dot lasers,” *IEEE J. Quantum Electron.* **54**, 1–7 (2018).
- <sup>13</sup>H. Huang, J. Duan, B. Dong, J. Norman, D. Jung, J. E. Bowers, and F. Grillot, “Epitaxial quantum dot lasers on silicon with high thermal stability and strong resistance to optical feedback,” *APL Photonics* **5**, 016103 (2020).
- <sup>14</sup>B. Dong, H. Huang, J. Duan, G. Kurczveil, D. Liang, R. G. Beausoleil, and F. Grillot, “Frequency comb dynamics of a 1.3  $\mu\text{m}$  hybrid-silicon quantum dot semiconductor laser with optical injection,” *Opt. Lett.* **44**, 5755–5758 (2019).
- <sup>15</sup>F. Cappelli, G. Villares, S. Riedi, and J. Faist, “Intrinsic linewidth of quantum cascade laser frequency combs,” *Optica* **2**, 836–840 (2015).
- <sup>16</sup>L. L. Columbo, S. Barbieri, C. Sirtori, and M. Brambilla, “Dynamics of a broadband quantum cascade laser: From chaos to coherent dynamics and mode-locking,” *Opt. Express* **26**, 2829–2847 (2018).
- <sup>17</sup>M. Piccardo and F. Capasso, “Laser frequency combs with fast gain recovery: Physics and applications,” *Laser Photonics Rev.* **16**, 2100403 (2022).
- <sup>18</sup>J. Duan, H. Huang, Z. G. Lu, P. J. Poole, C. Wang, and F. Grillot, “Narrow spectral linewidth in InAs/InP quantum dot distributed feedback lasers,” *Appl. Phys. Lett.* **112**, 121102 (2018).
- <sup>19</sup>F. Grillot, W. W. Chow, B. Dong, S. Ding, H. Huang, and J. Bowers, “Multimode physics in the mode locking of semiconductor quantum dot lasers,” *Appl. Sci.* **12**, 3504 (2022).
- <sup>20</sup>J. Faist, G. Villares, G. Scalari, M. Rösch, C. Bonzon, A. Hugi, and M. Beck, “Quantum cascade laser frequency combs,” *Nanophotonics* **5**, 272–291 (2016).
- <sup>21</sup>P. Bardella, L. L. Columbo, and M. Gioannini, “Self-generation of optical frequency comb in single section quantum dot fabry-perot lasers: A theoretical study,” *Opt. Express* **25**, 26234–26252 (2017).
- <sup>22</sup>J.-Z. Huang, Z.-T. Ji, J.-J. Chen, W.-Q. Wei, J.-L. Qin, Z.-H. Wang, Z.-Y. Li, T. Wang, X. Xiao, and J.-J. Zhang, “Ultra-broadband flat-top quantum dot comb lasers,” *Photonics Res.* **10**, 1308 (2022).
- <sup>23</sup>M. Heydari, A. R. Zali, R. E. Gildeh, and A. Farmani, “Fully integrated, 80 GHz bandwidth, 1.3  $\mu\text{m}$  InAs/InGaAs CW-PW quantum dot passively colliding-pulse mode-locked (CPM) lasers for IR sensing application,” *IEEE Sens. J.* **22**, 6528–6535 (2022).

- <sup>24</sup>S. Bischoff, J. Mørk, T. Franck, S. D. Brorson, M. Hofmann, K. Fröjdh, L. Prip, and M. P. Sørensen, "Monolithic colliding pulse mode-locked semiconductor lasers," *Quantum Semiclassical Opt.: J. Eur. Opt. Soc. Part B* **9**, 655 (1997).
- <sup>25</sup>G. Kurczveil, A. Descos, D. Liang, M. Fiorentino, and R. Beausoleil, "Hybrid silicon quantum dot comb laser with record wide comb width," in *Frontiers in Optics/Laser Science* (OSA, Washington, D.C., 2020), p. FTu6E.6.
- <sup>26</sup>G. Kurczveil, D. Liang, M. Fiorentino, and R. G. Beausoleil, "Robust hybrid quantum dot laser for integrated silicon photonics," *Opt. Express* **24**, 16167 (2016).
- <sup>27</sup>C. Silvestri, X. Qi, T. Taimre, K. Bertling, and A. D. Rakić, "Frequency combs in quantum cascade lasers: An overview of modeling and experiments," *APL Photonics* **8**, 020902 (2023).
- <sup>28</sup>F. Lelarge, B. Rousseau, B. Dagens, F. Poingt, F. Pommereau, and A. Accard, "Room temperature continuous-wave operation of buried ridge stripe lasers using InAs-InP (100) quantum dots as active core," *IEEE Photonics Technol. Lett.* **17**, 1369–1371 (2005).
- <sup>29</sup>B. Zhao, T. R. Chen, S. Wu, Y. H. Zhuang, Y. Yamada, and A. Yariv, "Direct measurement of linewidth enhancement factors in quantum well lasers of different quantum well barrier heights," *Appl. Phys. Lett.* **62**, 1591 (1993).
- <sup>30</sup>H. Huang, K. Schires, P. J. Poole, and F. Grillot, "Non-degenerate four-wave mixing in an optically injection-locked InAs/InP quantum dot Fabry-Perot laser," *Appl. Phys. Lett.* **106**, 143501 (2015).
- <sup>31</sup>C. Silvestri, L. L. Columbo, M. Brambilla, and M. Gioannini, "Coherent multi-mode dynamics in a quantum cascade laser: Amplitude- and frequency-modulated optical frequency combs," *Opt. Express* **28**, 23846–23861 (2020).
- <sup>32</sup>P. Glas, M. Naumann, A. Schirmacher, L. Däweritz, and R. Hey, "Self pulsing versus self locking in a CW pumped neodymium doped double clad fiber laser," *Opt. Commun.* **161**, 345–358 (1999).
- <sup>33</sup>C. Silvestri, "Theory and modelization of quantum cascade laser dynamics: Comb formation, field structures and feedback-based imaging," Ph.D. thesis, Politecnico di Torino, 2022.
- <sup>34</sup>A. G. Vladimirov and D. Turaev, "Model for passive mode locking in semiconductor lasers," *Phys. Rev. A* **72**, 033808 (2005).
- <sup>35</sup>R. Raghunathan, A. de Pinho e Braga, M. T. Crowley, J. K. Mee, and L. F. Lester, "Dynamics of split-pulsing in a two-section passively mode locked quantum dot laser," in *proceedings of CLEO*, San Jose, CA (IEEE, 2013), pp. 1–2.